Energy-band-structure study of the ZrN(100) surface

A. Callenås and L. I. Johansson
Department of Physics and Measurement Technology, Linköping University, S-581 83 Linköping, Sweden

A. N. Christensen
Department of Chemistry, Aarhus University, DK-8000 Aarhus C, Denmark

K. Schwarz, P. Blaha, and J. Redinger
Institute of Technical Electrochemistry, Technical University of Vienna, Getreidemarkt 9, A. 1060 Vienna, Austria
(Received 27 December 1983)

Results of angle-resolved-photoemission measurements made on the (100) surface of a $ZrN_{0.93}$ crystal are reported together with the results of a linear augmented-plane-wave band-structure calculation made for $ZrN_{1.0}$. The calculated band structure is used to interpret the experimental data and a good agreement between calculated and experimental band locations and dispersions is obtained. A *Tamm* surface state is also identified on ZrN(100).

I. INTRODUCTION

Transition-metal nitrides and carbides show many interesting physical and electrical properties,[1] such as extremely high melting points, extreme hardness, and metallic conductivity. Some of these materials are even superconductors with transition temperature up to 18 K. These properties are related to the electronic structure of the materials. Detailed studies of the electronic structure of transition-metal nitrides therefore seem well motivated, and below we present the results of angle-resolved-photoemission (ARPES) experiments and of a band-structure calculation on ZrN. By using the ARPES technique on a single-crystal ZrN sample and the results of a band-structure calculation, the individual energy bands could be identified and their location and dispersion could be determined experimentally. Earlier photoemission studies[2,3] on ZrN were carried out on polycrystalline samples, which only provide information about the total density of occupied states.

Both angle-resolved-photoemission results from a ZrN(100) crystal and the results of a linear augmented-plane-wave (LAPW) band-structure calculation, carried out to final-state energies of about 40 eV above the Fermi level, are reported. The calculation was made for the stoichiometric composition $ZrN_{1.0}$, while the experiments were made on a nonstoichiometric crystal, $ZrN_{0.93}$. The band-structure calculation is used to interpret the experimental results within the direct-transition model. The applicability of the direct-transition model to nonstoichiometric compounds has been demonstrated earlier on TiN(100) (Ref. 4) and TiC(100) (Ref. 5) crystals. It is found to work well also in this study of ZrN(100) since most of the structures observed in the photoemission spectra can be interpreted as originating from direct bulk band transitions. The existence of a surface-induced state at about 3.5 eV below the Fermi level in the normal-emission spectra from ZrN(100) is also reported.

II. EXPERIMENTAL

Angle-resolved-photoemission measurements have been performed by using resonance radiation from a differentially pumped uv lamp (He I and Ne I radiation; 21.2 and 16.85 eV, respectively). The emitted electrons were energy analyzed with a movable hemispherical electrostatic analyzer, having an acceptance "cone" represented by a rectangle of dimensions $\pm 1°$ by $\pm 3°$. The energy resolution of the energy analyzer was about 0.2 eV. The spectrometer had a base pressure of less than 1×10^{-10} Torr.

A single crystal of ZrN was made by the zone-annealing technique.[6] A Zr rod of nominal 99.99% purity was zone annealed in a 99.99%-nitrogen atmosphere under a pressure of 2 MPa. The temperature was approximately 2800 °C in the zone. The composition of the crystal $ZrN_{0.93}$ was determined gravimetrically as ZrO_2 obtained by ignition of ZrN in air at 1180 °C.

The ZrN(100) crystal which has rocksalt structure, was cleaned *in situ* by high-temperature flashings. Flashings to about 1300 °C were found to produce a clean surface. To maintain a clean surface during measurement, high-temperature flashings about once every 3 h were necessary. The cleanliness of the sample was checked with Auger electron spectroscopy.

The crystal was oriented azimuthally prior to mounting in the spectrometer with the aid of x-ray diffraction and the channeling pattern observed in a scanning electron microscope. In the spectra shown below, the incidence angle of the radiation θ_i and the electron-emission angle θ_e are given relative to the sample surface normal. The midpoint of the Fermi edge is used as the reference level for all spectra.

III. RESULTS AND DISCUSSION

A. Band-structure calculation

For the present analysis we need the energy bands of $ZrN_{1.0}$ up to 40 eV above the Fermi level. Since none of

the available band-structures exist up to sufficiently high energies and on a sufficiently fine $\vec{k}$ grid, we performed new calculations based on the self-consistent $X\alpha$ crystal potential given by Schwart *et al.*[7] The energies were calculated for a plane through the Brillouin zone surrounded by the $\vec{k}$ points Γ-(Δ)-*X*-*U*-*L*-*K*-(Σ)-Γ. In this plane a uniform mesh of 149 $\vec{k}$ points is obtained by dividing the Δ direction into 16 and the Σ direction into 12 intervals.

The actual computation was done in three steps: First we used the fully symmetrized augmented plane wave (APW) method[8] to extend the band structure up to the desired energies for high-symmetry $\vec{k}$ points. In the second step the LAPW (Ref. 9) was employed to check the accuracy of the linearization in comparison with the APW eigenvalues. In previous cases[4] it was found that the linearization is adequate over an energy range of about 1 Ry. Four energy regions were required to span the whole energy range of interest. The parameters E_l (for definition see Ref. 9) for the radial wave functions inside the atomic spheres are given in Table I. This choice of parameters gives an agreement of the band energies between the LAPW and APW method to within a few millirydbergs for the lower-energy regions. For the high-energy region, where *f* bands appear, deviations of up to about 20 mRy occur. This, however, is not caused by the linearization, but rather by the limitation of the LAPW expansion to 140 plane waves.

In contrast to TiC and TiN, relativistic effects are no longer negligible for ZrN but they are still sufficiently small that they can be treated by the approximate technique of Koelling and Harmon,[10] in which the dirac equation is solved by dropping the spin-orbit interaction. Thus in the third step we obtain the band energies for all $\vec{k}$ points of the chosen grid by using this pseudorelativistic LAPW method. The relativistic corrections leave some energies unchanged, but lower others by as much as 65 mRy especially for some of the Zr *s* band (Darwin *s* shift). By combining the LAPW eigenvalues from the four energy sheets and by using the symmetrized APW results together with the compatibility relations, we obtained the complete band structure shown in Fig. 1.

TABLE I. Energy parameters for the pseudorelativistic LAPW calculations. E_{sep} separates the different energy regions; E_l^t is the energy around which the *l*-like radial wave functions inside atomic sphere *t* are expanded. All energies are with respect to the muffin-tin zero.

Region	E_{sep}	E_l
1		N sphere: $E_l=0.5$ Ry except $E_s^N=-0.3$ Ry
		Zr sphere: $E_l=0.7$ Ry except $E_p^{Zr}=0.0$ Ry
	1.05 Ry	
2		All $E_l=1.4$ Ry
	1.75 Ry	
3		All $E_l=2.2$ Ry
	2.60 Ry	
4		All $E_l=2.9$ Ry except $E_f^{Zr}=3.2$ Ry

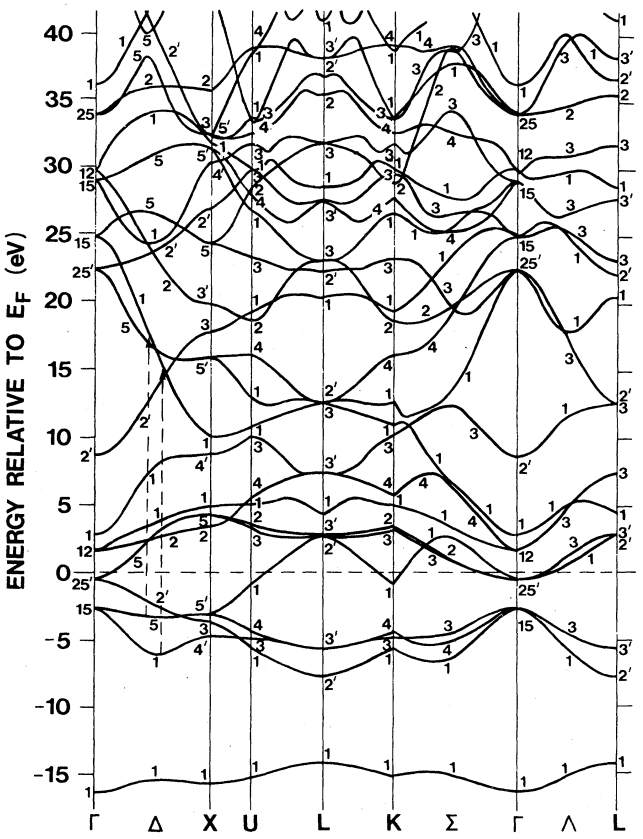

FIG. 1. Band structure of $ZrN_{1.0}$ using the LAPW method. Direct transitions for 21.2-eV radiation at normal emission from the (100) surface are illustrated by the dashed arrows (peaks *C* and *D* in Fig. 2).

B. Experimental results

Angle-resolved electron-energy distribution curves (EDC's) recorded at different polar angles θ_e, along the $\langle 011 \rangle$ azimuth using unpolarized He I (21.2-eV) radiation are shown in Fig. 2. The spectra are normalized to a constant peak height of the dominant structure. For the spectra shown in Fig. 2(a), the incidence angle θ_i is 15°, while it is 45° for those shown in Fig. 2(b). When comparing the normal-emission spectra in Figs. 2(a) and 2(b) a strong polarization effect is observed for the peaks labeled *B*, *C*, and *D*. From the observed polarization dependence, the symmetry of the initial states can be identified. Since peak *D*, at about −6.3 eV, is larger for $\theta_i=45°$ than for $\theta_i=15°$ it can according to symmetry-selection rules[11] be identified as arising from initial states of Δ_1 symmetry. The two peaks *B* and *C* are more intense at $\theta_i=15°$ than at $\theta_i=45°$ and can therefore be associated with emission from a Δ_5 initial-state band.

Peak *C*, at about −4.1 eV, shows a strong dispersion as a function of the polar angle. By using the direct-transition model and the band-structure calculation, this peak can be interpreted as arising from transitions between the initial-state band of Δ_5 symmetry at about 3.5 eV below the Fermi level and the final-state band of Δ_1

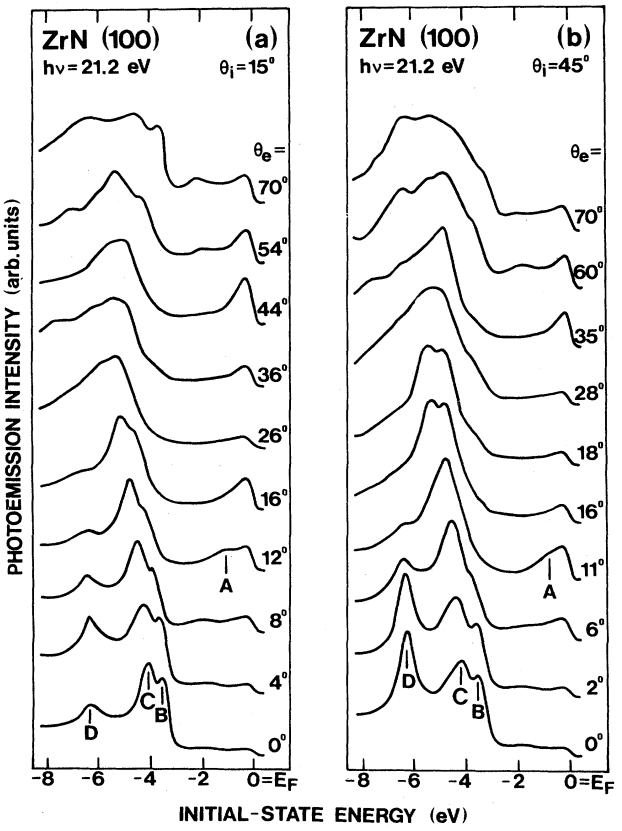

FIG. 2. Angle-resolved EDC's from ZrN(100) measured at various polar angles θ_e using unpolarized HeI radiation. (a) $\theta_i = 15°$ and (b) $\theta_i = 45°$.

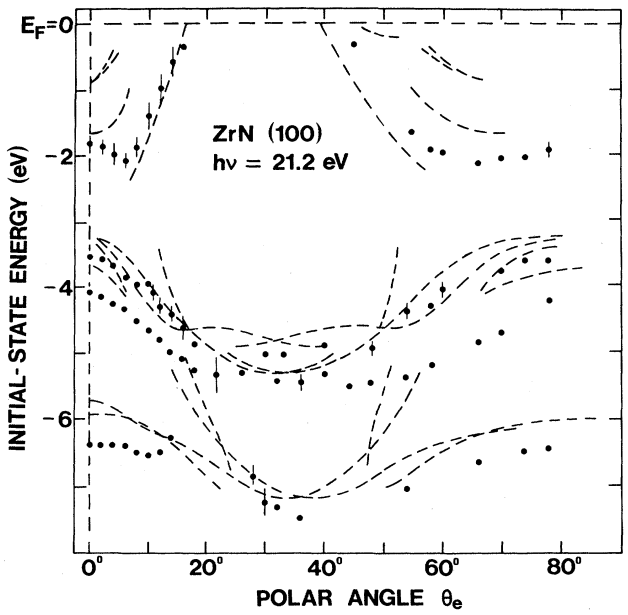

FIG. 3. Comparison between experimental and calculated peak positions as functions of polar angles along the ⟨011⟩ azimuth. See text for details.

symmetry at about 17.7 eV above the Fermi level, $\Delta_5(E_F - 3.5$ eV$) \rightarrow \Delta_1(E_F + 17.7$ eV) (see dashed arrow along the $\Gamma \rightarrow X$ symmetry line in Fig. 1).

Peak D corresponds to transitions between the Δ_1 initial-state band at about 6.0 eV below E_F and the final-state band of Δ_1 symmetry at about 15.2 eV above E_F, $\Delta_1(E_F - 6.0$ eV$) \rightarrow \Delta_1(E_F + 15.2$ eV). (See dashed arrows in Fig. 1.)

Transitions from the initial band of $\Delta_{2'}$ symmetry to the final band of Δ_1 symmetry, $\Delta_{2'}(E_F - 1.8$ eV$) \rightarrow \Delta_1(E_F + 19.4$ eV), are believed to give rise to peak A. According to symmetry-selection rules, emission from the $\Delta_{2'}$ band is forbidden at normal electron emission, but due to the finite acceptance angle of the analyzer used, a weak structure is expected to be observed. The selection rules may, however, explain why peak A is seen to become stronger upon increasing the polar angle.

In Fig. 2 peak B, at about -3.5 eV, cannot be accounted for by direct transitions between bulk energy bands. This peak is interpreted as originating from a surface-induced state, which will be discussed later in this paper and in a forthcoming publication.

In Fig. 3 the energy positions of peaks A, B, C, and D are plotted versus polar angle. The vertical bars on the data points indicate the estimated uncertainty in the determination of peak positions (when larger than ± 0.1 eV). The calculated dispersions are shown as dashed lines.

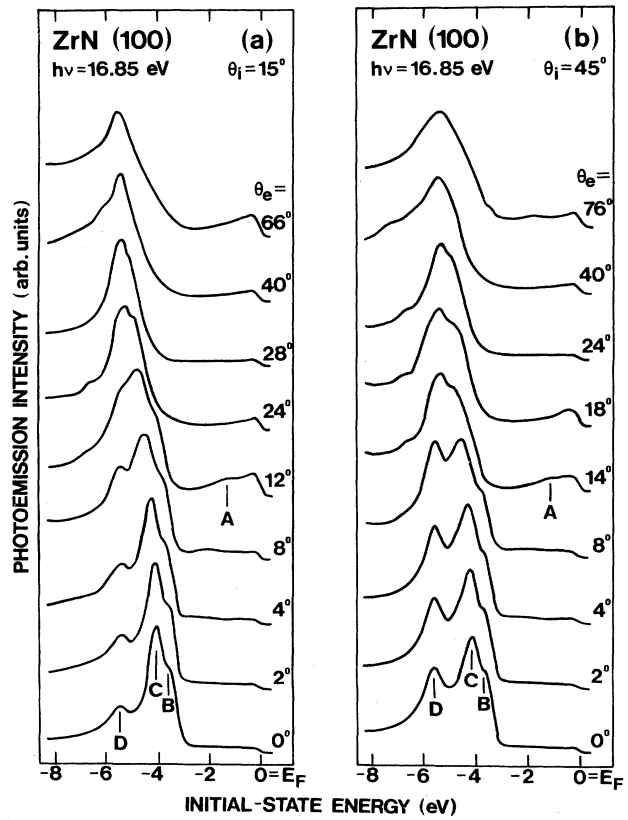

FIG. 4. Angle-resolved EDC's from ZrN(100) measured at various polar angles θ_e using unpolarized NeI radiation. (a) $\theta_i = 15°$ and (b) $\theta_i = 45°$.

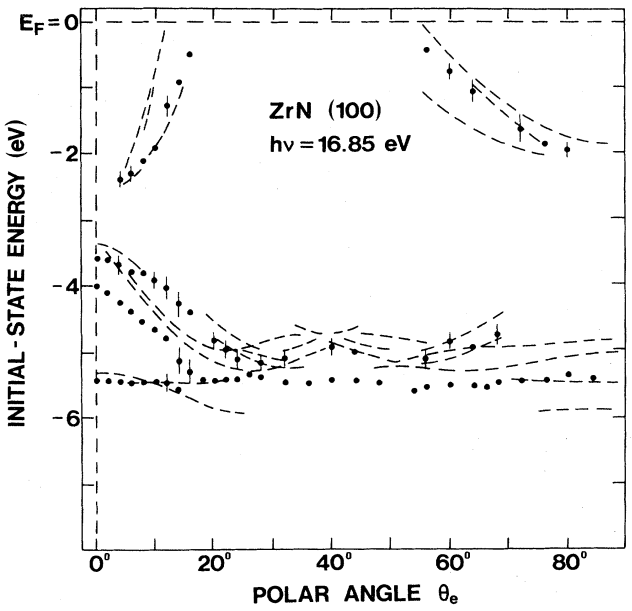

FIG. 5. Comparison between experimental and calculated peak positions as functions of polar angles along the ⟨011⟩ azimuth. See text for details.

These results were obtained from the full band structure using the same method as in previous papers.[4,5] The calculated and the experimental results agree fairly well. The major difference is that the calculated bands, corresponding to peaks *C* and *D*, lie about 0.5 eV closer to the Fermi level than the experimental results.

Figure 4 shows EDC's recorded at different polar angles along the ⟨011⟩ azimuth, using unpolarized Ne I (16.85-eV) radiation. By using the polarization dependence, symmetry-selection rules, and the band-structure calculation in the same way as for He I radiation, the peaks in Fig. 4 can be identified unambiguously. Peaks *C* and *D* are interpreted as associated with transitions $\Delta_5(E_F-3.4$ eV$)\rightarrow\Delta_1(E_F+13.5$ eV) and $\Delta_1(E_F-5.3$ eV$)\rightarrow\Delta_1(E_F+11.5$ eV), respectively. Peak *B* as originating from the surface-induced state mentioned above. Emission from the initial-state band of $\Delta_{2'}$ symmetry is not seen in the normal-emission spectrum, but appears as peak *A* in the off-normal-emission spectra.

In Fig. 5 the energy positions of the peaks shown in Fig. 4 are plotted versus polar angle. Also shown in Fig. 5 are the calculated dispersions illustrated as dashed lines. The agreement between the experimental and calculated results is fairly good even at this photon energy. The dots corresponding to peak *C*, however, lie 0.5 eV deeper below the Fermi level than the calculated positions.

C. Discussion

All the structures observed in the photoemission spectra, shown in Figs. 2 and 4, from the (100) surface of the $ZrN_{0.93}$ crystal can be identified unambiguously. Except for peak *B* all the structures can be explained in terms of direct transitions between calculated bulk bands. Along the $\Gamma\rightarrow X$ symmetry line, the final-state band is of Δ_1 symmetry and is located between 10 and 25 eV above E_F; see Fig. 1. The applicability of the direct-transition model to nonstoichiometric transition-metal compounds has been demonstrated earlier for TiN(100) (Ref. 4) and TiC(100).[5] Even for these compounds there is a similar Δ_1 final-state band along the $\Gamma\rightarrow X$ symmetry line. In the photoemission spectra from TiC(110) and TiC(111) surfaces, on the other hand, strong three-dimensional density-of-states features were observed,[5] together with direct bulk band transitions, and this was attributed to a lack of appropriate final-state bands in these directions for the photon energies used.

In Figs. 3 and 5 the experimental peak positions plotted as a function of polar angle are compared with calculated band dispersions. Considering that this is the first band mapping reported on ZrN, good agreement between the experimental and calculated results is obtained. Differences of up to 0.5 eV are seen, however, and the trend is the same as observed earlier for TiN(100),[4] namely, that the experimental results locate the bands somewhat deeper below E_F than the calculated values. It is evident from the calculated dispersions shown in Figs. 3 and 5 that several final-state bands, of different symmetries along $\Gamma\rightarrow X$ in Fig. 1, can contribute at off-normal emission. For determining which final-state bands do give the dominant contributions among the different possible branches, a calculation of transition probabilities needs to be carried out. Such a calculation has not yet been made, but it is now possible to calculate the photocurrent from ZrN(100) using the recently developed extended version[12] of the scheme based on the time-reversed low-energy electron diffraction theory.[13]

The peaks labeled *B* and *C* in Figs. 2 and 4 exhibit a strong polarization dependence. Peak *B*, which cannot be identified with bulk band transitions, shows the same polarization dependence as peak *C*, which is interpreted as due to emission from the initial-state band of Δ_5 symmetry. This suggests that peak *B* is closely associated with the Δ_5 band. The Δ_5 band, around -3.5 eV in Fig. 1, is doubly degenerated and its electronic structure can be described as pd_π bands between N *p* and Zr *d* orbitals (of t_{2g} symmetry) as discussed[14] for TiC. In transition-metal nitrides there is a charge transfer[8] from the transition metal to nitrogen. If this charge transfer persists at the surface, the change in the number of nearest neighbors at the surface will lead to a change in the potential at the surface. This change would cause an upward shift in the energy levels at the N atoms which may be sufficiently large to pull a *Tamm* surface state off the Δ_5 band. For TiN(100) the potential change has been calculated[15] and found to be sufficiently large, and calculated photoemission spectra[16] also give strong evidence of a *Tamm* surface state. Since the surface state on TiN(100) looked very much the same as peak *B* in the normal-emission spectra shown in Figs. 2 and 4, peak *B* is interpreted as a *Tamm* surface state on ZrN(100).

IV. SUMMARY

The locations and dispersions of the energy bands for a ZrN(100) crystal have been mapped out by using the

angle-resolved-photoemission technique and the results of a LAPW band-structure calculation, and by applying the direct-transition model. A good overall agreement was obtained between calculated and experimental results, considering this is the first detailed band mapping made on ZrN. The applicability of the direct-transition model for band mapping on transition-metal nitrides of nonstoichiometric composition has again been demonstrated.

A peak in the photoemission spectra from the ZrN(100) surface was interpreted as due to a surface-induced state. Such a surface-induced state has previously been observed on TiN(100).[17] In order to obtain more information about the electronic structure of transition-metal nitrides, similar studies are now being performed on VN(100) and NbN(100).

ACKNOWLEDGMENTS

This research has been financially supported by the Swedish Natural Research Council. The band-structure computations were performed at Interfakultäres Rechenzentrum der Technischen Universität Wien.

[1]L. E. Toth, *Transition Metal Carbides and Nitrides* (Academic, New York, 1971).
[2]H. Höchst, R. D. Bringans, P. Steiner, and Th. Wolf, Phys. Rev. B 25, 7183 (1982).
[3]W. K. Schubert, R. N. Schelton, and E. L. Wolf, Phys. Rev. B 24, 6278 (1981).
[4]L. I. Johansson, A. Callenås, P. M. Stefan, A. N. Christensen, and K. Schwarz, Phys. Rev. B 24, 1883 (1981).
[5]A. Callenås, L. I. Johansson, A. N. Christensen, K. Schwarz, and J. Redinger, Phys. Rev. B 27, 5934 (1983).
[6]A. N. Christensen, J. Cryst. Growth 33, 99 (1976).
[7]K. Schwarz, H. Ripplinger, and A. Neckel, Z. Phys. B 48, 79 (1982).
[8]A. Neckel, P. Rastl, R. Eibler, P. Weinberger, and K. Schwarz, J. Phys. C 9, 579 (1976).
[9]O. K. Andersen, Phys. Rev. B 12, 3060 (1976); D. D. Koelling and G. O. Arbman, J. Phys. C 10, 3107 (1977).
[10]D. D. Koelling and B. N. Harmon, J. Phys. C 10, 3107 (1977).
[11]J. Hermanson, Solid State Commun. 22, 9 (1977).
[12]C. G. Larsson, Ph.D. thesis, Chalmers University of Technology, Gothenburg, 1982, ISBN 91-7032-078-0.
[13]J. F. L. Hopkinson, J. B. Pendry, and D. J. Titterington, Comput. Phys. Commun. 19, 69 (1980).
[14]P. Blaha and K. Schwarz, Int. J. Quantum Chem. 23, 1535 (1983).
[15]J. E. Inglesfield, A. Callenås, and L. I. Johansson, Solid State Commun. 44, 1321 (1982).
[16]C. G. Larsson, L. I. Johansson, and A. Callenås, Solid State Commun. 49, 727 (1984).
[17]L. I. Johansson and A. Callenås, Solid State Commun. 42, 299 (1982).